Fluorescence intensity and squeezing in a driven three-level atom: Ladder case

Z. Ficek,[1] B. J. Dalton,[1,2] and P. L. Knight[2]
[1]*Department of Physics, The University of Queensland, Brisbane, Queensland 4072, Australia*
[2]*Optics Section, Blackett Laboratory, Imperial College of Science, Technology and Medicine, Prince Consort Road, London SW7 2BZ, United Kingdom*
(Received 27 December 1993)

A theoretical study is made of the steady-state intensity and squeezing properties of the fluorescent light from a three-level-atom system in a ladder configuration, which is subject to spontaneous-emission decay to the electromagnetic-field vacuum. Two cases are examined: in the equispaced (ES) level case, the two atomic transition frequencies are nearly equal and two photon absorption processes occur from a single coherent laser field that couples both transitions and has a small detuning from each; in the non-equispaced (NES) level case, the atomic transition frequencies are rather different and two photon absorption processes occur from two coherent laser fields, each coupled to a single transition and in near resonance with it. In both cases, a situation of small two-photon detuning occurs. Optical Bloch equations for the atomic density matrix in rotating frames are given and matrix expressions for determining the steady-state populations and coherences are obtained. Analytic expressions are also given for special cases. The fluorescent intensity is obtained from the populations of the intermediate and upper states, with the normally ordered variance (NOV) for quadrature components of the fluorescent field involving, in addition, the atomic coherences. The fluorescent intensities are shown graphically as a function of two-photon detuning for a variety of one-photon detunings and Rabi frequencies for the ES and NES cases. In both cases, the fluorescent intensities show the well known resonances from the upper state at zero two-photon detuning and from the intermediate state at zero one-photon detuning for the lower transition. However, further resonances are also found. The intermediate-state intensity displays a resonance at zero two-photon detuning. Also, the upper-state intensity shows a resonance at zero one-photon detuning for the upper transition, but only for the NES case; evidently, the transfer rate from upper to lower transition coherences destroys this resonance for the ES case. The time-averaged NOV is also shown graphically as a function of two-photon detuning for a variety of one-photon detunings and Rabi frequencies for the ES and NES cases. For the ES case, the quadrature frequency is chosen as the single laser frequency and for the NES case, it is chosen as either the average of the two laser frequencies or the lower transition laser frequency. Squeezing occurs near zero two-photon detuning for both ES and NES cases, though only for the quadrature frequency equal to the average laser frequency in the latter case. It also occurs near zero detuning for the lower transition for both cases, though only for the quadrature frequency equal to the lower transition laser frequency in the NES case. The squeezing minima show a splitting effect for large Rabi frequencies corresponding to two-photon or one-photon Rabi splitting of the dressed atom levels for the situation near two-photon or one-photon resonance, respectively. The large squeezing near two-photon resonance for moderate Rabi frequencies and large one-photon detuning corresponds to essentially pure three-level squeezing, while that near one-photon resonance for weak Rabi frequencies involves two-level squeezing.

PACS number(s): 42.50.Dv

I. INTRODUCTION

There is a large number of theoretical and experimental studies that have been made on the subject of two-photon absorption by three-level atoms in ladder, vee, and lambda configurations, interacting with one or two coherent laser fields. References [1–18] list some of these together with reviews covering aspects of this subject. For the ladder configuration which is the subject of the present paper, phenomena involving two-photon absorption lead to a resonance in the population of the upper states for zero two-photon detuning, even when the two one-photon absorptions involved are well off resonance. The particular interest of such a process consists of the possibility of studying excited states whose dipole matrix elements with the ground state are zero. In certain cases [3,19,20], this process can lead to a population inversion between the ground and upper excited states that could be useful in the realization of a two-photon laser. Two-photon correlated emission lasers [21–23] based on coherent excitation of a three-level ladder system, for example by two coherent laser fields, have been proposed and are predicted to generate squeezed light. Two-photon lasers operating at optical frequencies [24–26] have been realized based on population inversion between certain pairs of dressed states. These are associated with a two-level atom driven by a strong single-mode field, but the physics essentially involves a hierarchy of ladder systems.

Different perturbative approaches have been used to

determine the population of the upper state in the three-level atom [1–9], which is a measure of the two-photon absorption probability. Perturbation solutions tend to be very complex beyond the lowest-order approximations and are only valid in certain parameter regimes, such as when the intensities of the driving fields are relatively low, and they do not describe saturation effects. However, strong driving-field intensities are required to make two-photon absorption significant, since the two-photon absorption probability scales as the intensity squared in the nonsaturation regime. In general, nonperturbative methods involving the solution of optical Bloch equations will be required. Experimentally, the two-photon absorption probability can be conveniently measured as the total fluorescence intensity from the upper state. As indicated above [1–18], the fluorescence intensity shows a resonant behavior with regard to the two-photon detuning with a maximum value on two-photon resonance and a half width determined by the width of the upper state. For the case of two driving laser fields, Salomaa [5] has shown that for intensities such that the Rabi frequencies and decay rates are comparable and with a large detuning of one laser from the lower transition frequency, two peaks appear in the upper-state fluorescence intensity profile: one when the second laser is on resonance with the upper transition frequency as well as the usual peak when the lasers are on two-photon resonance. Kieu and Dalton [27] considered a four-level system, with one upper state and two intermediate states. The results can be specialized to the ladder system by making certain Rabi frequencies and decay rates zero. They find that not only the upper state, but also the intermediate states, exhibit a resonance behavior centered on zero two-photon detuning, the intermediate state resonance being due to spontaneous-emission processes from the upper state following resonant two-photon absorption.

In this paper, we make a detailed study of two-photon absorption in a three-level ladder system, concentrating on the squeezing properties of the fluorescent field as well as on its intensity. In one case (*equispaced*, ES) the atomic transition frequencies are approximately equal and the atom is driven by *one* laser field, which couples to both transitions and has a small one-photon detuning from each. In the other more usual case (*nonequispaced*, NES) the atomic transition frequencies are rather different and the atom is driven by *two* laser fields, each of which is coupled to one transition only and from which it has a small one-photon detuning. In both cases, the laser fields are also close to two-photon resonance. In our model, spontaneous-emission decay from the upper excited state to the intermediate state and thence to the lower state occurs and is thus restricted to the levels within the ladder system. In real atoms, the situation would be more complicated and the simple three-state model would need to be extended to allow for other decay channels, laser-field couplings between various magnetic substates, and so on. The model also does not allow for Doppler effects, although Doppler-free situations can be realized experimentally be applying the technique of trapping single ions in a Paul trap [28]. Extensions of our simple model to allow for real-atom effects, although necessary in later work to describe actual experiments, at this stage would tend to obscure the basic physical effects described in this paper.

The previous work emphasizes effects of two-photon absorption on the populations of the excited states. The fluorescent intensity is treated in terms of the populations of the intermediate and upper states of the ladder system. In this paper, we emphasize the effects on atomic coherences that are reflected in the squeezing properties of the fluorescence field. As we will see, both one- and two-photon coherences will be important. In this paper, we discuss squeezing in terms of the variance of quadrature components of the total electric field [29] rather than in terms of the squeezing spectrum [30]. The latter, which involves an experimental realization where the field is frequency filtered and then homodyned with a local oscillator field, is used in many squeezing experiments. The former involves an experimental process in which the total field is homodyned with the local oscillator field without first frequency filtering. Although more difficult experimentally, in this approach the squeezing properties of the total field would show up as sub-Poissonian statistics in the combined field, as has been outlined by Mandel [29(a)]. The squeezing spectrum and the total field squeezing give different information about the phase-dependent noise in the electric field. As both are, in principle, measurable we prefer here to use the total field squeezing as being more closely related to the fundamental definition of what "squeezing" means in terms of variances of the total field quadrature components, where a basic Heisenberg uncertainty principle relationship applies to quadrature components whose phases differ by $\pi/2$ [29]. Squeezing associated with ladder systems has been previously discussed in the context of the two-photon correlated emission laser [21–23], where an excitation process that generated atomic coherence between the outer states of the ladder can result in squeezed light in one- or two-mode laser cavity fields. Reversible spontaneous emission into one- or two-mode cavity fields from coherently excited single-atom ladder systems has also been treated [31,32] in a generalized Jaynes-Cummings model approach and squeezed-light fields obtained. No previous study of squeezing in the fluorescent light emitted from ladder systems in empty space seems to exist. Squeezing in resonance fluorescence has been predicted for two-level atoms [29(a),33–35], three-level atoms of the lambda type [36–38], and for the vee type [39]. In two-level atoms, the steady-state squeezing is restricted to a weak-driving-field regime, whereas in three-level lambda systems the squeezing appears for weak as well as for moderate intensities of the driving fields. For three-level atoms of the lambda type, the steady-state fluorescence squeezing that was shown appears when the decay rates to the two lower states and the Rabi frequencies are different. For these parameters, a single one-photon coherence and the two-photon coherence are significantly nonzero, and the squeezing has what shall be referred to as a *two-level–three-level-atom* character [40].

In a related work on squeezing for three-level atoms of lambda, vee, and ladder configurations [40], we have considered the general question of classifying the types of

squeezing (Fig. 9 below) that can occur for the light field emitted from such three-level sources. This classification is, of course, based on considering the squeezing in the total field, where the variance of quadrature components involves one-time correlation functions that can be related to populations and coherences of the atomic sources. It would not apply to the squeezing spectrum [30], where two-time correlation functions are involved. We have obtained results for the optimum or largest squeezing that can occur irrespective of the choice of quadrature component, and allowing for *all* possible states in which the atom could be. For the particular process of resonance fluorescence studied here for ladder systems, the amount of squeezing would be, in general, less than for this optimum case. In terms of this general analysis, we can see that for lambda systems no purely three-level-atom squeezing (in which only the two-photon coherences are nonzero) can occur [40], basically since they do not appear explicitly in the expression for the normally ordered variance, and the one-photon coherences need to be nonzero if it is to become negative. However, for ladder systems, it is possible that the squeezing could be of a purely *three-level-atom* type, since, as we will see below, the two-photon coherences appear in the phase-dependent terms of the normally ordered variance.

With appropriate selection of atomic parameters, we will find cases of the resonance fluorescence from three-level atoms in the ladder configuration exhibiting close to pure three-level-atom squeezing. Not only do the two-photon coherences appear in the expressions for the variance of the quadrature components, but they are also significantly nonzero. Cases of essentially pure two-level squeezing are also found. For an arbitrary choice of frequency for the quadrature component, the variances oscillate even at long times. However, for the case of equispaced levels driven by one-laser field, choosing a quadrature component frequency the same as that of the driving field will result in a time-independent variance after a long time. For the case of nonequispaced levels driven by two-laser fields, no choice of quadrature frequency produces time-independent variances at long times. However, if the quadrature frequency is chosen either equal to the average of the driving laser frequencies or equal to one of them, then the long time variance contains a time-independent component plus high-frequency oscillating components whose time average is zero. Such time averaging of the long time variances corresponds to a process that could be carried out on the time-dependent experimental results and has the effect of removing uninteresting transient and oscillating effects. It cannot, of course, lead to squeezing at long times when none previously existed; indeed, negative swings in the time-dependent variance of the quadrature components would tend to be averaged out.

This paper is organized as follows. Optical Bloch equations for a three-level atom in the ladder configuration and driven by the single-mode or two-mode laser field are described in Sec. II. The fluorescent intensity is examined in Sec. III for a variety of parameter regimes. Squeezing of the fluorescence field is studied in Sec. IV and a discussion is given in the concluding Sec. V.

II. OPTICAL BLOCH EQUATIONS

We consider a three-level system (Fig. 1) which in the case of nearly *equispaced* levels [Fig. 1(a)] is driven by a single linearly polarized monochromatic laser field of frequency ω_L coupled to both the $1\rightarrow 2$ and $2\rightarrow 3$ transitions, and which in the case of *nonequispaced* levels [Fig. 1(b)] is driven by two linearly polarized monochromatic laser fields of frequencies ω_a and ω_b coupled to the $1\rightarrow 2$ and $2\rightarrow 3$ transitions, respectively. In all cases the fields are not far from both one-photon and two-photon resonance. The transition frequencies between the ground state $|1\rangle$ and the intermediate state $|2\rangle$, and between the state $|2\rangle$ and the upper state $|3\rangle$, are ω_1 and ω_2, respectively. These transitions are associated with electric-dipole matrix elements μ_1 and μ_2, respectively (assumed real for simplicity), whereas the $1\rightarrow 3$ transition is forbidden in the electric-dipole approximation. Spontaneous-

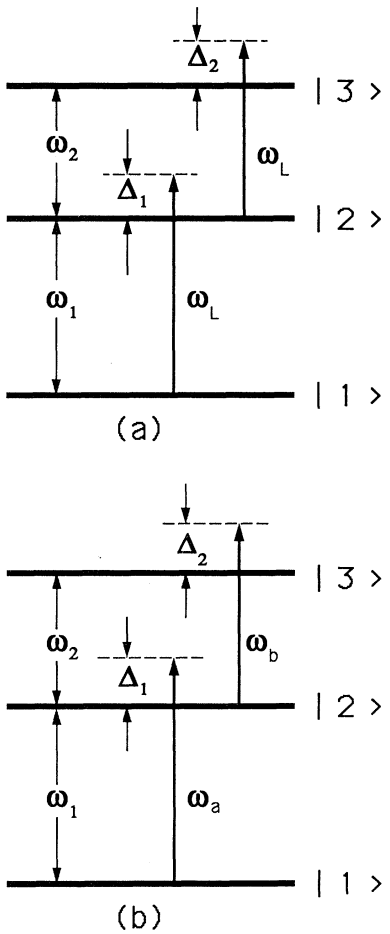

FIG. 1. (a) Three-level atom in a ladder configuration with nearly equispaced levels driven by a coherent laser field of frequency ω_L detuned from the atomic transition frequencies by $\Delta_1=\omega_L-\omega_1$ and $\Delta_2=\omega_L-\omega_2$. (b) Three-level atom in a ladder configuration with nonequispaced levels driven by two coherent fields of frequencies ω_a,ω_b detuned from the atomic transition frequencies by $\Delta_1=\omega_a-\omega_1$ and $\Delta_2=\omega_b-\omega_2$.

emission decays to an empty vacuum via the simple downward cascade $|3\rangle\rightarrow|2\rangle\rightarrow|1\rangle$ occur with decay rates Γ_{22} and Γ_{11}, respectively. The nearly equispaced and nonequispaced level cases are distinguished by $|\omega_1-\omega_2|$ being much smaller than, or comparable to, a typical optical frequency, respectively.

Our aim is to calculate the steady-state populations and coherences of the atomic states and thus the squeezing properties of the fluorescence field. The master equation for the reduced density operator ρ of the three-level atom describes its evolution in the external laser driving fields (treated classically) along with the effects of spontaneous emission and is given [41] in the interaction picture by

$$\frac{\partial\rho'}{\partial t}=-\frac{i}{\hbar}[H_I',\rho']-\frac{1}{2}\sum_{i,j=1}^{2}\Gamma_{ij}(\rho' S_i^+ S_j^- + S_i^+ S_j^-\rho' - 2S_j^-\rho' S_i^+)e^{i(\omega_i-\omega_j)t}, \tag{1}$$

where the prime denotes the interaction picture for the operators. In Eq. (1), $S_i^+=|i+1\rangle\langle i|$ and $S_i^-=(S_i^+)^\dagger$ $(i=1,2)$ are transition operators. The coherence transfer rate $\Gamma_{12}=\Gamma_{21}$ which couples the $2\rightarrow3$ to the $1\rightarrow2$ atomic coherences is given by [3,19,41]

$$\Gamma_{21}=\frac{\boldsymbol{\mu}_2\cdot\boldsymbol{\mu}_1^*}{6\pi\varepsilon_0\hbar c^3}(\omega_2^3+\omega_1^3) \tag{2}$$

and is zero when $\boldsymbol{\mu}_1$ and $\boldsymbol{\mu}_2$ are orthogonal.

In both cases, Rabi frequencies, detunings, and relaxation rates $[\Gamma_{21}\sim(\Gamma_{11}\Gamma_{22})^{1/2}]$ are small compared to optical frequencies and are similar in magnitude. Evaluation of Γ_{21} produces the following selection rules in terms of angular momentum quantum numbers: $\Delta(J_1 1 J_2)$, $\Delta(J_2 1 J_3)$, and $M_3-M_2=M_2-M_1=\pm1,0$. The Γ_{21} terms can be ignored in the case of nonequispaced levels via the application of the rotating-wave approximation of the second kind (adiabatic approximation) [41,42] since they couple coherences whose frequencies differ by much more than an optical frequency. However, for the case of nearly equispaced levels, these terms cannot be ignored. In Eq. (1), H_I' is the interaction Hamiltonian between the atom and the driving field(s), given in the dipole and rotating-wave approximation as follows.

For the ES level case,

$$H_I'=-\tfrac{1}{2}i\hbar\Omega_1(S_1^+e^{-i\Delta_1 t}e^{-i\phi_L}-S_1^-e^{i\Delta_1 t}e^{i\phi_L}) -\tfrac{1}{2}i\hbar\Omega_2(S_2^+e^{-i\Delta_2 t}e^{-i\phi_L}-S_2^-e^{i\Delta_2 t}e^{i\phi_L}), \tag{3}$$

where the laser electric field is $E_0\sin(\omega_L t+\phi_L)$, which has an amplitude $\mathbf{E}_0$ and a phase ϕ_L, $\Delta_i=\omega_L-\omega_i$ $(i=1,2)$ are the one-photon detunings and $\Omega_i=\boldsymbol{\mu}_i\cdot\mathbf{E}_0/\hbar$ $(i=1,2)$ are the Rabi frequencies. This laser field could be described quantum mechanically via a coherent state $|\alpha_L\rangle$ for the mode of frequency ω_L, linear polarization $\mathbf{e}_L$, with $\alpha_L=\sqrt{\bar{n}_L}e^{-i\phi_L}$ and $\mathbf{E}_0=(2\hbar\omega_L\bar{n}_L/\varepsilon_0 V)^{1/2}\mathbf{e}_L$.

For the NES level case,

$$H_I'=-\tfrac{1}{2}i\hbar\Omega_1(S_1^+e^{-i\Delta_1 t}e^{-i\phi_a}-S_1^-e^{i\Delta_1 t}e^{i\phi_a}) -\tfrac{1}{2}i\hbar\Omega_2(S_2^+e^{-i\Delta_2 t}e^{-i\phi_b}-S_2^-e^{i\Delta_2 t}e^{i\phi_b}), \tag{4}$$

where the laser electric field is $\mathbf{E}_{a0}\sin(\omega_a t+\phi_a)+\mathbf{E}_{b0}\sin(\omega_b t+\phi_b)$ involving amplitudes $\mathbf{E}_{a0}$, $\mathbf{E}_{b0}$ and phases ϕ_a, ϕ_b for the two frequency components, $\Delta_1=(\omega_a-\omega_1)$ and $\Delta_2=(\omega_b-\omega_2)$ are the one-photon detunings between the laser fields and their coupled atomic transition frequencies, and $\Omega_1=\boldsymbol{\mu}_1\cdot\mathbf{E}_{a0}/\hbar$ and $\Omega_2=\boldsymbol{\mu}_2\cdot\mathbf{E}_{b0}/\hbar$ are the Rabi frequencies. This laser field could be described quantum mechanically as a product of coherent states $|\alpha_a\rangle|\alpha_b\rangle$ for the two modes of frequencies ω_a, ω_b and linear polarizations $\mathbf{e}_a$, $\mathbf{e}_b$, with $\alpha_c=\sqrt{\bar{n}_c}e^{-i\phi_c}$ and $\mathbf{E}_{c0}=(2\hbar\omega_c\bar{n}_c/\varepsilon_0 V)^{1/2}\mathbf{e}_c$ $(c=a,b)$.

The matrix elements of ρ' according to Eq. (1) satisfy linear coupled equations of motion containing explicit time-dependent factors of the complex exponential type. These can be removed using the following transformations:

(a) For the ES level case,

$$\begin{aligned}
&\sigma_{ii}=\rho_{ii}'=\rho_{ii}\ ,\quad i=1,2,3\ ,\\
&\sigma_{23}=e^{-i\phi_L}e^{-i\Delta_2 t}\rho_{23}'=e^{-i\phi_L}e^{-i\omega_L t}\rho_{23}=\sigma_{32}^*\ ,\\
&\sigma_{12}=e^{-i\phi_L}e^{-i\Delta_1 t}\rho_{12}'=e^{-i\phi_L}e^{-i\omega_L t}\rho_{12}=\sigma_{21}^*\ ,\\
&\sigma_{13}=e^{-2i\phi_L}e^{-i(\Delta_1+\Delta_2)t}\rho_{13}'\\
&\quad=e^{-2i\phi_L}e^{-2i\omega_L t}\rho_{13}=\sigma_{31}^*\ .
\end{aligned} \tag{5}$$

(b) For the NES level case,

$$\begin{aligned}
&\sigma_{ii}=\rho_{ii}'=\rho_{ii}\ ,\quad i=1,2,3\ ,\\
&\sigma_{23}=e^{-i\phi_b}e^{-i\Delta_2 t}\rho_{23}'=e^{-i\phi_b}e^{-i\omega_b t}\rho_{23}=\sigma_{32}^*\ ,\\
&\sigma_{12}=e^{-i\phi_a}e^{-i\Delta_1 t}\rho_{12}'=e^{-i\phi_a}e^{-i\omega_a t}\rho_{12}=\sigma_{21}^*\ ,\\
&\sigma_{13}=e^{-i(\phi_a+\phi_b)}e^{-i(\Delta_1+\Delta_2)t}\rho_{13}'\\
&\quad=e^{-i(\phi_a+\phi_b)}e^{-i(\omega_a+\omega_b)t}\rho_{13}=\sigma_{31}^*\ .
\end{aligned} \tag{6}$$

In terms of the σ_{ij}, the Bloch equations are almost exactly the same for both the nearly equispaced and the nonequispaced cases, differing only due to the coherence transfer rate Γ_{21}. The equations may be written in simple form using suitable scaled variables

$$\begin{aligned}
&\tau=(\Gamma_{11}+\Gamma_{22})t\ ,\quad \gamma_1=\frac{\Gamma_{11}}{\Gamma_{11}+\Gamma_{22}}\ ,\\
&\gamma_2=\frac{\Gamma_{22}}{\Gamma_{11}+\Gamma_{22}}\ ,\quad \gamma_{21}=\frac{\Gamma_{21}}{\Gamma_{11}+\Gamma_{22}}\ ,\\
&\xi_1=\frac{\Omega_1}{\Gamma_{11}+\Gamma_{22}}\ ,\quad \xi_2=\frac{\Omega_2}{\Gamma_{11}+\Gamma_{22}}\ ,\\
&\Delta=\frac{\Delta_1+\Delta_2}{\Gamma_{11}+\Gamma_{22}}\ ,\quad \delta=\frac{\Delta_2-\Delta_1}{\Gamma_{11}+\Gamma_{22}}\ .
\end{aligned} \tag{7}$$

In these scaled variables τ is the scaled time, γ_1, γ_2,γ_{21} are scaled relaxation rates, ξ_1, ξ_2 are scaled Rabi frequen-

cies, Δ is the scaled two-photon detuning, and δ is the difference between the scaled one-photon detunings.

The Bloch equations are for the ES level case

$$\begin{aligned}
\frac{\partial\sigma_{33}}{\partial\tau} &= -\gamma_2\sigma_{33}-\tfrac{1}{2}\xi_2(\sigma_{23}+\sigma_{32}) , \\
\frac{\partial\sigma_{22}}{\partial\tau} &= \gamma_2\sigma_{33}-\gamma_1\sigma_{22}-\tfrac{1}{2}\xi_1(\sigma_{12}+\sigma_{21})+\tfrac{1}{2}\xi_2(\sigma_{23}+\sigma_{32}) , \\
\frac{\partial\sigma_{11}}{\partial\tau} &= \gamma_1\sigma_{22}+\tfrac{1}{2}\xi_1(\sigma_{12}+\sigma_{21}) , \\
\frac{\partial\sigma_{23}}{\partial\tau} &= -\tfrac{1}{2}[1+i(\Delta+\delta)]\sigma_{23}-\tfrac{1}{2}\xi_1\sigma_{13} \\
&\quad +\tfrac{1}{2}\xi_2(\sigma_{33}+\sigma_{22}) , \\
\frac{\partial\sigma_{12}}{\partial\tau} &= -\tfrac{1}{2}[\gamma_1+i(\Delta-\delta)]\sigma_{12}+\tfrac{1}{2}\xi_1(\sigma_{22}-\sigma_{11}) \\
&\quad +\tfrac{1}{2}\xi_2\sigma_{13}+\gamma_{21}\sigma_{23} , \\
\frac{\partial\sigma_{13}}{\partial\tau} &= -(\tfrac{1}{2}\gamma_2+i\Delta)\sigma_{13}+\tfrac{1}{2}\xi_1\sigma_{23}-\tfrac{1}{2}\xi_2\sigma_{12} ,
\end{aligned} \tag{8}$$

and for the NES level case

$$\frac{\partial\sigma_{12}}{\partial\tau} = -\tfrac{1}{2}[\gamma_1+i(\Delta-\delta)]\sigma_{12}+\tfrac{1}{2}\xi_1(\sigma_{22}-\sigma_{11})+\tfrac{1}{2}\xi_2\sigma_{13} , \tag{9}$$

with all the other equations the same as in Eq. (8). The equations for σ_{32}, σ_{21}, and σ_{31} can be obtained from Eqs. (8) and (9) by complex conjugation. In the case of nearly equispaced levels, the inclusion of two driving fields of different frequencies, both of which would be coupled to both the $1\rightarrow2$ and $2\rightarrow3$ transitions, would lead to Bloch equations with additional terms and for which the time dependence could not be transformed away on account of the coherence transfer rate Γ_{21}. The presence of such an explicit time dependence in the Bloch equations will be considered in a later publication. The numerical techniques used in the present paper for solving the Bloch equations involve using the result that $\sigma_{11}+\sigma_{22}+\sigma_{33}$ equals unity to convert the Bloch equations (8) and (9) into eight linear inhomogeneous equations for the remaining density matrix elements (six coherences and two populations). The steady-state solutions can then be found by setting the time derivatives to zero and using matrix inversion techniques. These steady-state solutions will then be used to study the populations and coherences of the atomic levels and thus the squeezing properties of the emitted fluorescence field.

III. FLUORESCENCE INTENSITY

Populations in the intermediate and upper states may be monitored experimentally in terms of the intensity of the fluorescent light emitted. In general, the populations considered as a function of the detuning Δ are not Lorentzian and in this section we study the resonance behavior of the driven three-level ladder system.

Simple analtyic solutions can be obtained for the case where the excited states have equal decay rates, $\Gamma_{11}=\Gamma_{22}$ and the Rabi frequencies are equal, $\Omega_1=\Omega_2$. Thus we have $\gamma_1=\gamma_2=\frac{1}{2}$ and $\xi_1=\xi_2=\xi$. For the nearly equispaced level case, we choose $\Gamma_{21}=\Gamma_{11}=\Gamma_{22}$ so that $\gamma_{21}=\frac{1}{2}$. In the nonequispaced level case, we have $\gamma_{21}=0$. Here the behavior is examined in various intensity regimes for the nearly equispaced level case.

In the weak-field limit ($\xi\ll1$) the populations are given by Lorentzians

$$\sigma_{33}(\infty)=\frac{\xi^4}{(\frac{1}{4}+4\Delta^2)[\frac{1}{4}+(\Delta-\delta)^2]} \tag{10}$$

and

$$\sigma_{22}(\infty)=\frac{\xi^2}{[\frac{1}{4}+(\Delta-\delta)^2]} \tag{11}$$

for the nearly equispaced level case and for all Δ,δ. This predicts that the population of the intermediate state shows resonance behavior when the detuning factors are equal, $\Delta\approx\delta$, corresponding to the one-photon resonance ($\Delta_1=0$) at the transition frequency $|1\rangle\rightarrow|2\rangle$. The population of the upper state, however, shows resonant behavior when the detunings are given by $\Delta=0$ and $\Delta=\delta$. The first case corresponds to two-photon resonance, the second case to resonance in the intermediate-state population through which a stepwise excitation to the upper state occurs. When the levels actually become equispaced, $\delta=0$, and the situation of two-photon resonance $\Delta=0$ coincides with the one-photon resonances at $\Delta=\delta$ and $\Delta=-\delta$.

Various other regimes can also be distinguished. At somewhat higher intensities we have

$$\sigma_{33}(\infty)=\frac{\xi^4}{(\frac{1}{4}+4\Delta^2)[\frac{1}{4}+2\xi^2+(\Delta-\delta)^2]} \tag{12}$$

and

$$\sigma_{22}(\infty)=\frac{\xi^4}{(\frac{1}{4}+4\Delta^2)[\frac{1}{4}+2\xi^2+(\Delta-\delta)^2]}+\frac{\xi^2}{[\frac{1}{4}+2\xi^2+(\Delta-\delta)^2]} . \tag{13}$$

This predicts that the one-photon resonance at $\Delta=\delta$ ($\Delta_1=0$) in both the intermediate and upper states is power broadened by the term $2\xi^2$. Also, the intermediate level is predicted to have a resonance at $\Delta=0$, zero two-photon detuning. This latter effect is due to the simultaneous absorption of two photons of frequencies $\omega_L=\omega_0=\frac{1}{2}(\omega_1+\omega_2)$ to cause the transition $|1\rangle\rightarrow|3\rangle$ followed by a spontaneous emission of a photon in conjunction with the $|3\rangle\rightarrow|2\rangle$ transition. For large one-photon detunings δ, the first term of (13) near $\Delta=0$ is approximately $\xi_4/\{\delta^2(\frac{1}{4}+4\Delta^2)\}$ with the factor ξ^2/δ acting as a two-photon Rabi frequency.

In the very strong-field regime we find that

$$\sigma_{33}(\infty)=\tfrac{1}{3} \tag{14}$$

and

$$\sigma_{22}(\infty)=\frac{1}{3}\ , \tag{15}$$

indicating that all three atomic states are equally populated.

The effects described above can be seen under appropriate parameter regimes, and similar discussions apply to the nonequispaced level case. However, the physical possibilities for this system with regard to possible resonances are much more complex than the previous restricted discussion implies. To discover this, we use the previously described numerical methods to display the features. Both the ES and NES cases are considered, highlighting any differences the additional coherence transfer rate γ_{21} produces. The effects of differing spontaneous decay rates γ_1,γ_2 can also be considered.

We begin with the analysis of the populations in the excited atomic states. There can be striking differences between the ES and NES cases. Figure 2 shows the intermediate-state population versus two-photon detuning for the decay rates $\gamma_1=\gamma_2=0.5$, detuning $\delta=5$, and for increasing equal Rabi frequencies $\xi_1=\xi_2=\xi$. Resonances at $\Delta=0$ and $\Delta=\delta$ are seen in both the ES and NES cases, but at higher Rabi frequencies the resonance at $\Delta=\delta$ is shifted more for the NES case. The resonance at zero two-photon detuning is in accordance with the work of Kieu and Dalton [27]. As the detuning δ increases, the resonances at $\Delta=0$ and $\Delta=\delta$ become more resolved and the population in the intermediate state shows two distinct Lorentzians. This is illustrated in Fig. 3, where the steady-state intermediate-state population $\sigma_{22}(\infty)$ is plotted as a function of two-photon detuning Δ for the ES case with the decay rates $\gamma_1=\gamma_2=0.5$, the coherence transfer rate $\gamma_{21}=0.5$, and the much larger detuning $\delta=50$ as compared to Fig. 2. Results for two equal Rabi frequencies $\xi_1=\xi_2=\xi$ are shown. It is seen that there are two distinct Lorentzians: a broad one centered at $\Delta=\delta$ (zero lower-transition detuning $\Delta_1=0$) and a narrow one centered at $\Delta=0$ (zero two-photon detuning). There is no resonance at $\Delta=-\delta$ (zero upper-transition detuning). For large detunings δ, however, almost identical graphs apply to the NES level case with $\gamma_{21}=0$ and are not shown.

A more interesting situation emerges as we consider the upper-state population $\sigma_{33}(\infty)$. Figure 4 shows the

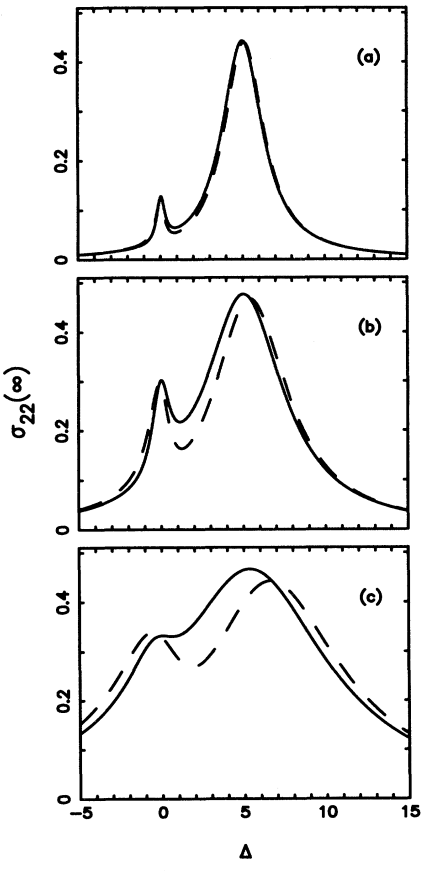

FIG. 2. The steady-state population $\sigma_{22}(\infty)$ of the intermediate state $|2\rangle$ as a function of two-photon detuning Δ for decay rates $\gamma_1=\gamma_2=0.5$, one-photon detuning $\delta=5$, and for various equal Rabi frequencies $\xi_1=\xi_2=\xi$. In (a) $\xi=1$, (b) $\xi=2$, and (c) $\xi=4$. For the ES level case (shown solid line), coherence transfer rate $\gamma_{21}=0.5$ and for the NES level case (shown dashed line), $\gamma_{21}=0$.

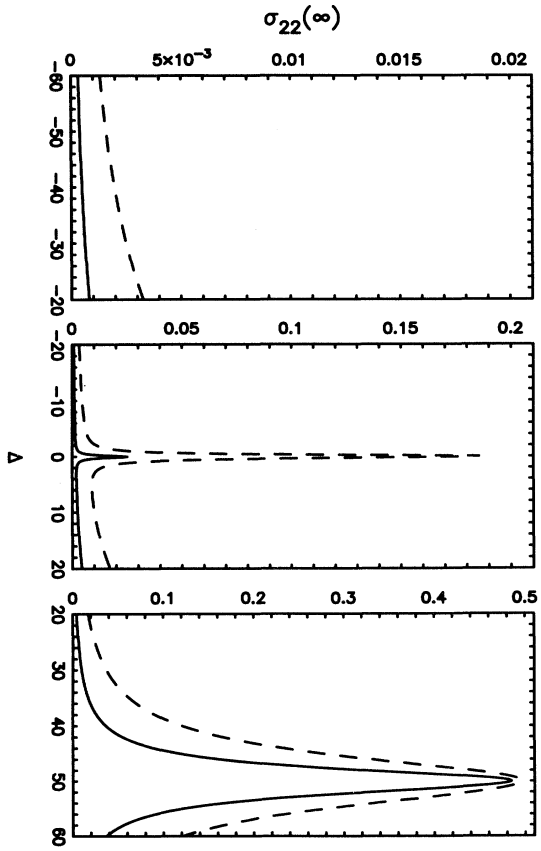

FIG. 3. The steady-state population $\sigma_{22}(\infty)$ of the intermediate state $|2\rangle$ as a function of two-photon detuning Δ for the ES level case with decay rates $\gamma_1=\gamma_2=0.5$, coherence transfer rate $\gamma_{21}=0.5$, and detuning $\delta=50$. Results for equal Rabi frequencies $\xi_1=\xi_2=\xi$ are shown for $\xi=2.0$ (solid line) and $\xi=4.0$ (dashed line).

steady-state population $\sigma_{33}(\infty)$ for the same parameters as in Fig. 2. For both the ES and NES cases, there is a strong resonance at $\Delta=0$, but only for a low intensity of the driving field ($\xi=0.2$) do we observe a weak resonance at $\Delta=\delta$. Power broadening tends to obscure the latter resonance. This resonance is significantly more pronounced for larger detuning δ. This is shown in Fig. 5, where the steady-state upper-state population $\sigma_{33}(\infty)$ is plotted versus two-photon detuning Δ for the same decay rates $\gamma_1=\gamma_2=0.5$ and detuning $\delta=50$ as applies to Fig. 3. Again, results for two equal Rabi frequencies, $\xi_1=\xi_2=\xi$, are shown. Figure 5 applies to the ES level case with $\gamma_{21}=0.5$ and shows results for the same ranges of detuning Δ as in Fig. 3. Now we see pronounced resonances at $\Delta=\delta$ (zero lower-transition detuning $\Delta_1=0$) and $\Delta=0$ (zero two-photon detuning), but no resonance for $\Delta=-\delta$ (zero upper-transition detuning $\Delta_2=0$). However, the NES level case with $\gamma_{21}=0$ in fact shows a resonance at $\Delta=-\delta$. This is illustrated in Fig. 6, where the steady-state population $\sigma_{33}(\infty)$ is plotted as a function of two-photon detuning Δ for the same parameters as in Fig. 5, but $\gamma_{21}=0$. It is seen that resonances at zero upper-transition detuning are indeed possible even though their occurrence is by no means apparent from analytic formulas. This is in accordance with the results of Salomaa [5]. The above graphs show that in the ES level case, the coherence transfer process due to γ_{21} destroys this effect.

When $\Gamma_{11}\neq\Gamma_{22}$ the resonant behaviors can be enhanced or diminished depending on the ratio $\alpha=\Gamma_{22}/\Gamma_{11}$. This is shown in Fig. 7, where we plot the steady-state population $\sigma_{22}(\infty)$ in the intermediate state $|2\rangle$ as a function of the two-photon detuning Δ for $\delta=5$, equal Rabi frequencies $\xi_1=\xi_2=\xi=2.0$, and different α. The normalized decay rates γ_1,γ_2 always satisfy $\gamma_1+\gamma_2=1$. Figure 7(a) is for $\alpha=10^{-2}$ and there appears a window instead of a peak in the population distribution at $\Delta=0$. This change in the behavior of the population in that state $|2\rangle$ is due to a population trapping in a coherent superposition of the upper state $|3\rangle$ and the lower state $|1\rangle$. The population is transferred to the state $|3\rangle$ by the absorption of two photons of the frequency ω_0 from the driving field, and is trapped in the superposition state due to its long lifetime, with only a small population

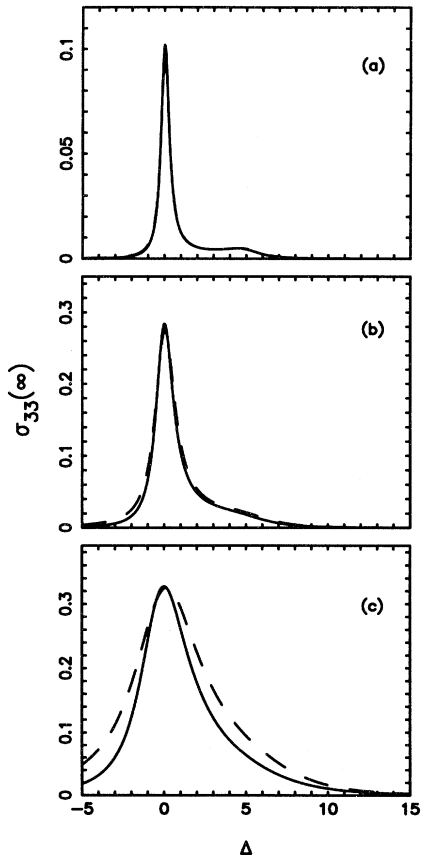

FIG. 4. The steady-state population $\sigma_{33}(\infty)$ of the upper state $|3\rangle$ as a function of two-photon detuning Δ for the decay rates $\gamma_1=\gamma_2=0.5$, one-photon detuning $\delta=5$, and for various equal Rabi frequencies $\xi_1=\xi_2=\xi$. In (a) $\xi=1$, (b) $\xi=2$, and (c) $\xi=4$. The ES level case with coherence transfer rate $\gamma_{21}=0.5$ is shown with a solid line and the NES level case with $\gamma_{21}=0$ is shown with a dashed line.

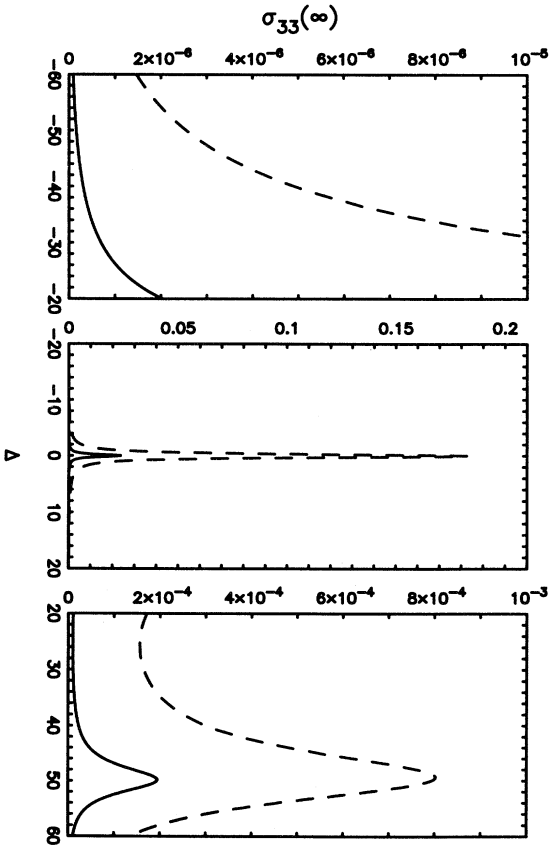

FIG. 5. The steady-state population $\sigma_{33}(\infty)$ of the upper state $|3\rangle$ as a function of two-photon detuning Δ for the ES level case, with decay rates $\gamma_1=\gamma_2=0.5$, coherence transfer rate $\gamma_{21}=0.5$, and detuning $\delta=50$. Results for equal Rabi frequencies $\xi_1=\xi_2=\xi$ are shown for $\xi=2.0$ (solid line) and $\xi=4.0$ (dashed line).

in $|2\rangle$. Figure 7(b) for $\alpha=1$ shows the familiar resonance at $\Delta=0$. For Fig. 7(c) with $\alpha=10^2$, the lifetime of the population in state $|3\rangle$ is very short, and we observe a pronounced peak in the population of the state $|2\rangle$centered at $\Delta=0$. Results for both the ES level case with $\gamma_{21}=(\gamma_1\gamma_2)^{1/2}$ and the NES level case with $\gamma_{21}=0$ are shown in Fig. 7, and both have similar behaviors.

The immediate consequence of population trapping in the superposition of the lower and upper states is the vanishing of the one-photon coherences 1-2 and 2-3 near $\Delta=0$. This is shown in Fig. 8, where the atomic coherences are plotted versus the two-photon detuning Δ for the same situation as in Fig. 7(a). Figure 8 corresponds to the ES level case, but the results for the NES level case are almost the same. The figure demonstrates the existence of a two-photon coherent population trapping, as the two-photon coherence 1-3 is large at the resonance $\Delta=0$, whereas the other one-photon coherences 1-2 and 2-3 vanish, along with the intermediate state population.

IV. SQUEEZING IN THE FLUORESCENCE FIELD

A. General squeezing expressions

A full discussion of the expressions used to describe squeezing is given in our basic paper, Ref. [40]. In the interest of brevity, only the key results will be given here.

The electric field operator $\hat{\mathbf{E}}$ can be written in terms of the quadrature components $\hat{\mathbf{E}}_\phi, \hat{\mathbf{E}}_{\phi-(\pi/2)}$ as [29]

$$\hat{\mathbf{E}}(\mathbf{R},t)=\hat{\mathbf{E}}_\phi\cos(\omega t-\mathbf{k}\cdot\mathbf{R}+\phi)+\hat{\mathbf{E}}_{\phi-(\pi/2)}\sin(\omega t-\mathbf{k}\cdot\mathbf{R}+\phi)\ . \tag{16}$$

The quadrature component of the electric field $\hat{\mathbf{E}}_\phi$ at frequency ω, wave vector $\mathbf{k}$, and phase ϕ is defined in terms of the positive and negative components $\hat{\mathbf{E}}^\pm$ as [29]

$$\hat{E}_\phi=\hat{E}^+e^{i\Phi}+\hat{E}^-e^{-i\Phi}\ , \tag{17}$$

where

$$\Phi=\omega t-\mathbf{k}\cdot\mathbf{R}+\phi\ , \tag{18}$$

and where we will generally interpret $\hat{E}^\pm$, $\hat{E}_\phi$, etc., as a specific vectorial component along vector $\mathbf{e}$, unless otherwise indicated. The operators $\hat{E}^\pm$, etc., are Heisenberg field operators at position $\mathbf{R}$ and time t.

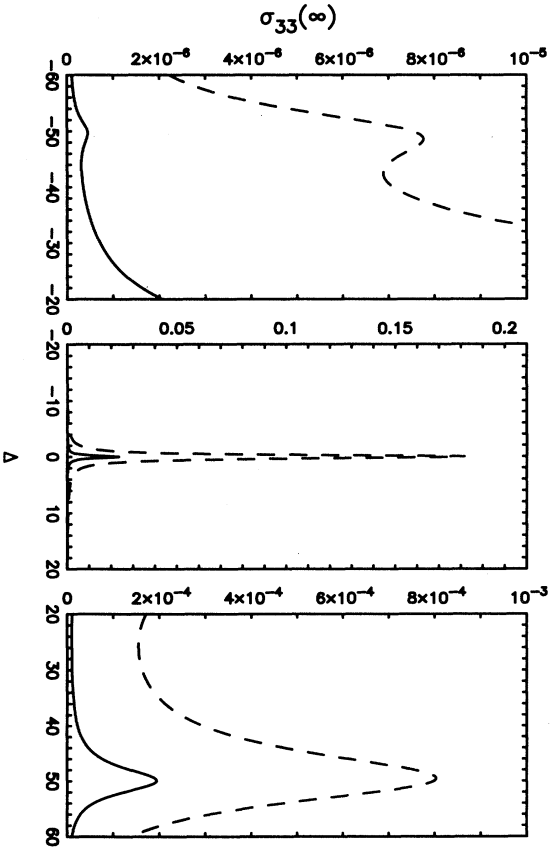

FIG. 6. The steady-state population $\sigma_{33}(\infty)$ of the upper state $|3\rangle$ as a function of two-photon detuning for the NES level case with decay rates $\gamma_1=\gamma_2=0.5$, coherence transfer rate $\gamma_{21}=0$, and detuning $\delta=50$.

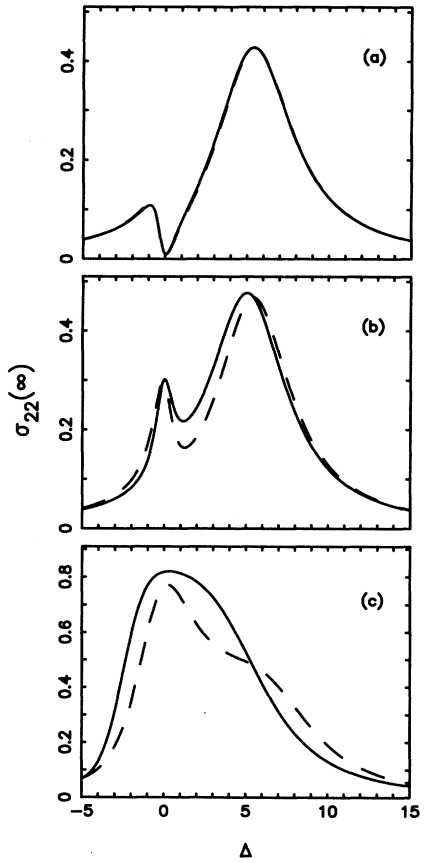

FIG. 7. The steady-state population $\sigma_{22}(\infty)$ of the intermediate state $|2\rangle$ as a function of two-photon detuning Δ for detuning $\delta=5$ and equal Rabi frequencies $\xi_1=\xi_2=\xi=2$. For various ratios of decay rates, the ES level case with $\gamma_{21}=\sqrt{\gamma_1\gamma_2}$ is shown (solid line) and the NES level case with $\gamma_{21}=0$ is shown (dashed line). The decay rates are such that $\gamma_1+\gamma_2=1$. In (a) $\alpha=\gamma_1/\gamma_2=10^{-2}$, in (b) $\alpha=1$, and in (c) $\alpha=10^2$.

The positive, negative frequency components can be written in terms of the modes λ for the quantum electromagnetic (EM) field as

$$\hat{\mathbf{E}}^{+}=\sum_{\lambda}\mathbf{f}_{\lambda}(\mathbf{R})\hat{a}_{\lambda} \tag{19}$$

$$=(\hat{\mathbf{E}}^{-})^{\dagger}\ , \tag{20}$$

where

$$\mathbf{f}_{\lambda}=i\left[\frac{\hbar\omega_{\lambda}}{2\varepsilon_0 V}\right]^{1/2}e^{i\mathbf{k}_{\lambda}\cdot\mathbf{R}}\mathbf{e}_{\lambda}\ , \tag{21}$$

and where mode λ has wave vector $\mathbf{k}_{\lambda}$, frequency ω_{λ}, and polarization vector $\mathbf{e}_{\lambda}$. $\hat{a}_{\lambda}$ and $\hat{a}_{\lambda}^{\dagger}$ are the annihilation, creation operators, obeying the usual Bose commutation rules. If there are source atoms present, the formal solutions of the Heisenberg equations of motion for the annihilation, creation operators will involve atomic operators.

The quadrature component $\hat{E}_{\phi}$ of the total EM field is said to be *squeezed* relative to the other quadrature component $\hat{E}_{\phi-(\pi/2)}$ if the variance $\langle\Delta\hat{E}_{\phi}^{2}\rangle$ is smaller than for the minimum uncertainty state with equal variances

$$\langle\Delta\hat{E}_{\phi}^{2}\rangle<|\langle[\hat{E}^{+},\hat{E}^{-}]\rangle|\ . \tag{22}$$

Here, the variances $\langle\Delta\hat{\Omega}^{2}\rangle$ and the mean $\langle\hat{\Omega}\rangle$ are defined as

$$\langle\Delta\hat{\Omega}^{2}\rangle=\mathrm{Tr}[(\hat{\Omega}-\langle\hat{\Omega}\rangle)^{2}\hat{W}(0)]\ , \tag{23}$$

$$\langle\hat{\Omega}\rangle=\mathrm{Tr}[\hat{\Omega}\hat{W}(0)]\ , \tag{24}$$

where $\hat{W}(0)$ is the initial density operator for the quantum EM field and its sources.

Note here that we are referring to squeezing in the *total field.* Measurements of such squeezing generally involve beating the field under study with a strong local oscillator field of frequency ω, wave vector $\mathbf{k}$, and phase ϕ—a homodyne or heterodyne experiment. This would, of course, be a difficult experiment but can, in principle, be carried out as described by Mandel [29a].

Again it must be emphasized that we do not calculate the so-called *squeezing spectrum* [30]. This quantity involves a preliminary frequency filtering of the total field and then a homodyne or heterodyne measurement. Although the squeezing spectrum is easier to measure and describes certain aspects of squeezing, it is not relevant to the squeezing in the total field that is studied here.

The criterion for squeezing is that the normally ordered variance must be negative,

$$\langle:\Delta\hat{E}_{\phi}^{2}:\rangle<0\ , \tag{25}$$

where the normally ordered variance of the quadrature component $\hat{E}_{\phi}$ is given by

$$\begin{aligned}\langle:\Delta\hat{E}_{\phi}^{2}:\rangle=&(\langle\hat{E}^{+2}\rangle-\langle\hat{E}^{+}\rangle^{2})e^{2i\Phi}\\&+(\langle\hat{E}^{-2}\rangle-\langle\hat{E}^{-}\rangle^{2})e^{-2i\Phi}\\&+2(\langle\hat{E}^{-}\hat{E}^{+}\rangle-\langle\hat{E}^{-}\rangle\langle\hat{E}^{+}\rangle)\ .\end{aligned} \tag{26}$$

The electric-field operator $\hat{\mathbf{E}}$ can then be expressed as the sum of a *free-field* term $\hat{\mathbf{E}}_F$ and a *source-field* term $\hat{\mathbf{E}}_S$ [41] given in the electric-dipole interaction approximation as

$$\hat{\mathbf{E}}=\hat{\mathbf{E}}_F+\hat{\mathbf{E}}_S\ , \tag{27}$$

where

$$\hat{\mathbf{E}}_F=\sum_{\lambda}\mathbf{f}_{\lambda}(\mathbf{R})\hat{a}_{\lambda}(0)e^{-i\omega_{\lambda}t}+\mathrm{H.c.}\ , \tag{28}$$

with $f_{\lambda}(\mathbf{R})$ given by (21), and

$$\hat{\mathbf{E}}_S=\nabla\times\left[\nabla\times\frac{1}{4\pi\varepsilon_0}\sum_{A}\frac{\hat{\boldsymbol{\mu}}_A[t-(|\mathbf{R}-\mathbf{R}_A|/c)]}{|\mathbf{R}-\mathbf{R}_A|}\times\theta\left[t-\frac{|\mathbf{R}-\mathbf{R}_A|}{c}\right]\right]\ . \tag{29}$$

For the source field, the sum in (29) is over different atoms A whose position is at $\mathbf{R}_A$ and whose electric-dipole operator is $\hat{\boldsymbol{\mu}}_A$. θ is the usual Heaviside function, zero for negative argument, unity for positive argument.

In the case where the atoms are driven by a field whose

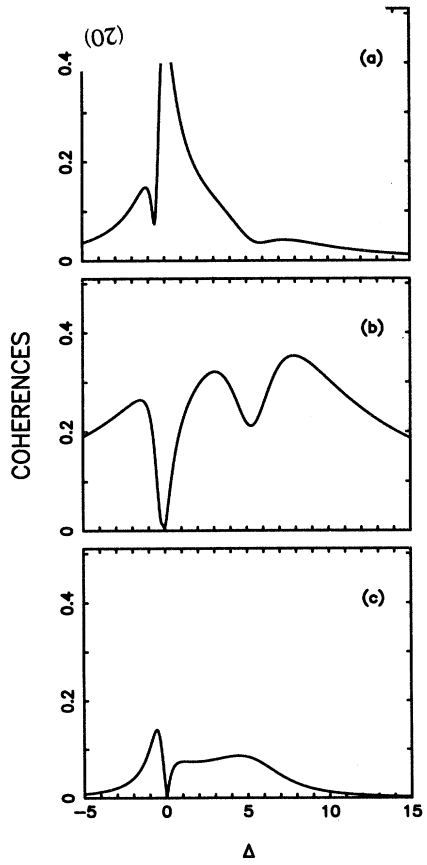

FIG. 8. The steady-state atomic coherences as a function of the two-photon detuning Δ for detuning $\delta=5$ and $\alpha=10^{-2}$ as in Fig. 7(a). The coherence $|\sigma_{13}|$ is shown in (a), $|\sigma_{12}|$ in (b), and $|\sigma_{23}|$ in (c). Only the ES level case is shown, since the results for the NES level case are almost the same.

classical amplitude is zero at the detector, and in the Dicke model situation where the atoms are all located within a region about the origin which is small compared to the transition wavelength, the normally ordered variance in the *total field* equals the normally ordered variance for the *source field* [40]. Squeezing for the total field hence requires the normally ordered variance for the source field to be negative. Thus

$$\langle :\Delta\hat{E}_{\phi}^{2}: \rangle = \langle :\Delta\hat{E}_{\phi S}^{2}: \rangle \ , \tag{30}$$

and

$$\langle \Delta\hat{E}_{\phi}^{2} \rangle = \langle :\Delta\hat{E}_{\phi S}^{2}: \rangle + \langle \Delta\hat{E}_{\phi}^{2} \rangle_{\text{coherent state}} \ , \tag{31}$$

with

$$\langle \Delta\hat{E}_{\phi}^{2} \rangle_{\text{coherent state}} = \sum_{\lambda} |\mathbf{f}_{\lambda}\cdot\mathbf{e}|^{2} \geq 0 \ . \tag{32}$$

The normally ordered variance $\langle :\Delta\hat{E}_{\phi S}^{2}: \rangle$ of the source field given by

$$\begin{aligned}\langle :\Delta\hat{E}_{\phi S}^{2}: \rangle = &(\langle \hat{E}_{S}^{+2} \rangle - \langle \hat{E}_{S}^{+} \rangle^{2}) e^{2i\Phi} \\ &+ (\langle \hat{E}_{S}^{-2} \rangle - \langle \hat{E}_{S}^{-} \rangle^{2}) e^{-2i\Phi} \\ &+ 2(\langle \hat{E}_{S}^{-}\hat{E}_{S}^{+} \rangle - \langle \hat{E}_{S}^{-} \rangle \langle \hat{E}_{S}^{+} \rangle) \ ,\end{aligned} \tag{33}$$

where $\hat{E}_{S}^{+}, \hat{E}_{S}^{-}$ are the positive, negative frequency components.

In the asymptotic regime where the field detectors are located, we can find that to a good approximation and correct to the lowest inverse power of the atom-detector distances $|\mathbf{R}-\mathbf{R}_{A}|$, for the component along a unit vector $\mathbf{e}$ which is perpendicular to $\mathbf{R}-\mathbf{R}_{A}$ and for $t > |\mathbf{R}-\mathbf{R}_{A}|/c$, the following expressions [41] for the positive and negative frequency components:

$$\hat{E}_{S}^{+} = \mathbf{e}\cdot\hat{\mathbf{E}}_{S}^{+} = \frac{1}{4\pi\varepsilon_{0}c^{2}} \sum_{\substack{A \\ i>j}} \frac{\omega_{ji}^{2}\mathbf{e}\cdot\mathbf{d}_{ji}\hat{\Lambda}_{ji}^{A}[t-(|\mathbf{R}-\mathbf{R}_{a}|/c)]}{|\mathbf{R}-\mathbf{R}_{A}|} \ , \tag{34}$$

$$\hat{E}_{S}^{-} = \mathbf{e}\cdot\hat{\mathbf{E}}_{S}^{-} = \frac{1}{4\pi\varepsilon_{0}c^{2}} \sum_{\substack{A \\ i>j}} \frac{\omega_{ij}^{2}\mathbf{e}\cdot\mathbf{d}_{ij}\hat{\Lambda}_{ij}^{A}[t-(|\mathbf{R}-\mathbf{R}_{A}|/c)]}{|\mathbf{R}-\mathbf{R}_{A}|} \ . \tag{35}$$

The $\hat{\Lambda}_{ij}^{A} = |i\rangle\langle j|$ are atomic transition operators and $\mathbf{d}_{ij} = \langle i|\hat{\mu}_{A}|j\rangle$ are dipole matrix elements of the electric dipole operator $\hat{\mu}_{A}$ for the A atom. The atomic states $|i\rangle, |j\rangle$ have energies $\hbar\omega_{i}, \hbar\omega_{j}$ and $i > j$ signifies that $\omega_{i} > \omega_{j}$. These expressions are to be used in the forthcoming treatment of the fields produced by the three-level atoms.

B. Three-level ladder system

For the case of a single three-level ladder system at $\mathbf{R}_{A}=0$ and, with dipole matrix elements $\langle 3|\hat{\mathbf{d}}\cdot\mathbf{e}|2\rangle, \langle 2|\hat{\mathbf{d}}\cdot\mathbf{e}|1\rangle$ assumed equal (μ), and the atomic transition frequencies ω_{2}, ω_{1} assumed approximately the same ($\bar{\omega}$), the source field is given by

$$\hat{E}_{S}^{+} = \kappa(\hat{\Lambda}_{23} + \hat{\Lambda}_{12}) \ , \tag{36}$$

with

$$\kappa = \bar{\omega}^{2}\mu/4\pi\varepsilon_{0}c^{2}R \ . \tag{37}$$

The retarded time $t - R/c$ is implicit in the transition operators. This expression is a special case of Eq. (34) and of the case treated in earlier work [40]. In the notation of [40] $c = s = 1/\sqrt{2}$, $\kappa = K/\sqrt{2}$ and $(\omega^{2}\mu) = \bar{\omega}^{2}\mu$. As we now consider a single-atom system, the superscript A will be dropped for simplicity.

The normally ordered variance for the $\hat{E}_{\phi S}$ quadrature component of the source field can then be evaluated using the results

$$\frac{\langle \hat{E}_{S}^{+2} \rangle}{\kappa^{2}} = \frac{\langle \hat{E}_{S}^{-2} \rangle^{*}}{\kappa^{2}} = \rho_{31} \ , \tag{38}$$

$$\frac{\langle \hat{E}_{S}^{+} \rangle}{\kappa} = \frac{\langle \hat{E}_{S}^{-} \rangle^{*}}{\kappa} = \rho_{32} + \rho_{21} \ , \tag{39}$$

$$\frac{\langle \hat{E}_{S}^{-}\hat{E}_{S}^{+} \rangle}{\kappa^{2}} = \rho_{33} + \rho_{22} \ , \tag{40}$$

in conjunction with (33), and with the transformations (5) and (6).

For the NES level case, we obtain

$$\begin{aligned}\frac{\langle :\Delta\hat{E}_{\phi S}^{2}: \rangle}{\kappa^{2}} = &[e^{-i(\phi_{a}+\phi_{b})}e^{-i(\omega_{a}+\omega_{b})t'}\sigma_{31} - (e^{-i\phi_{b}}e^{-i\omega_{b}t'}\sigma_{32} + e^{-i\phi_{a}}e^{-i\omega_{a}t'}\sigma_{21})^{2}]e^{2i\Phi} \\ &+ [e^{i(\phi_{a}+\phi_{b})}e^{i(\omega_{a}+\omega_{b})t'}\sigma_{13} - (e^{i\phi_{b}}e^{i\omega_{b}t'}\sigma_{23} + e^{i\phi_{a}}e^{i\omega_{a}t'}\sigma_{12})^{2}]e^{-2i\Phi} \\ &+ 2[\sigma_{33} + \sigma_{22} - |(e^{-i\phi_{b}}e^{-i\omega_{b}t'}\sigma_{32} + e^{-i\phi_{a}}e^{-i\omega_{a}t'}\sigma_{21})|^{2}] \ ,\end{aligned} \tag{41}$$

where $t' = t - R/c$, and t' is implicit in the density matrix elements σ_{ij}. For the ES level case, $\phi_{a}, \phi_{b} \to \phi_{L}$ and $\omega_{a}, \omega_{b} \to \omega_{L}$ in (41). In both cases, the normally ordered variance contains oscillating terms. As $\Phi = \omega t - \mathbf{k}\cdot\mathbf{R} + \phi$, the time-independent part of the quadrature phase ϕ dependence will be of the form $e^{\pm 2i[\phi - (1/2)(\phi_{a}+\phi_{b}) - \mathbf{k}\cdot\mathbf{R}]}$ for the NES case and $e^{\pm 2i(\phi - \phi_{L} - \mathbf{k}\cdot\mathbf{R})}$ for the ES case.

Choosing the quadrature wave vector $\mathbf{k}$ along $\mathbf{R}$ gives $\mathbf{k}\cdot\mathbf{R}=\omega R/c$, so that all the time dependence involves the retarded time t'.

Time averaging over a suitably long time interval is carried out for the normally ordered variance, removing uninteresting oscillatory terms and transient effects. It must be emphasized that such time averaging does not, of course, create squeezing in the steady state where it does not occur. The time-averaged normally ordered variance is then optimized with respect to the quadrature phase ϕ. The quadrature frequency ω is then suitably chosen to optimize the prospects of obtaining squeezing.

For the ES level case, time averaging the normally ordered variance over the interval 0 to T ($T\gg\Gamma_{ij}^{-1}$) and optimizing the choice of quadrature phase ϕ gives

$$\left[\frac{\overline{\langle:\Delta E_{\varphi S}^2:\rangle}}{\kappa^2}\right]_{\text{opt}\phi}=-2|\sigma_{31}-(\sigma_{32}+\sigma_{21})^2|\times\left|\frac{\sin(\omega-\omega_L)T}{(\omega-\omega_L)T}\right|+2(\sigma_{33}+\sigma_{22}-|\sigma_{32}+\sigma_{21}|^2)\ , \quad (42)$$

where the σ_{ij} will be the steady-state values $\sigma_{ij}(\infty)$. This expression is a well behaved function of the time interval length T and the difference frequency $(\omega-\omega_L)$. Optimizing with respect to ϕ first, then time averaging, produces a different result, since the optimum ϕ depends on $(\omega-\omega_L)t'$.

For $\omega\neq\omega_L$, the choice of a long observation interval $T\gg|(\omega-\omega_L)|^{-1}$ (associated with the well known experimental time-frequency uncertainty principle) results in the first term becoming essentially zero, leaving behind the second term which is positive and hence cannot give rise to squeezing. On the other hand, for $\omega=\omega_L$, the modulus of the last factor or in the first term is equal to unity for all T, resulting in a negative term that could produce squeezing. Similar considerations apply in the NES level case.

In the ES level case and with $\omega=\omega_L$, the time-averaged optimized normally ordered variance is

$$\left[\frac{\overline{\langle:\Delta\hat{E}_{\phi S}^2:\rangle}}{\kappa^2}\right]_{\text{opt}\phi}=-2|\sigma_{31}-(\sigma_{32}+\sigma_{21})^2|+2(\sigma_{33}+\sigma_{22}-|\sigma_{32}+\sigma_{21}|^2)\ . \quad (43)$$

Both one- and two-photon coherences are involved.

For the NES level case and with $\omega=\frac{1}{2}(\omega_a+\omega_b)$, the time-averaged optimized normally ordered variance is

$$\left[\frac{\overline{\langle:\Delta\hat{E}_{\phi S}^2:\rangle}}{\kappa^2}\right]_{\text{opt}\phi}=-2|\sigma_{31}-2\sigma_{32}\sigma_{21}|+2(\sigma_{33}+\sigma_{22}-|\sigma_{32}|^2-|\sigma_{21}|^2)\ , \quad (44)$$

and for $\omega=\omega_a$,

$$\left[\frac{\overline{\langle:\Delta\hat{E}_{\phi S}^2:\rangle}}{\kappa^2}\right]_{\text{opt}\phi}=2(\sigma_{22}-2|\sigma_{21}|^2)+2(\sigma_{33}-|\sigma_{32}|^2)\ . \quad (45)$$

Note the involvement of the two-photon coherence σ_{31} for the $\omega=\frac{1}{2}(\omega_a+\omega_b)$ case but only one-photon coherences for the $\omega=\omega_a$ case.

For the ladder case, alternative descriptions of the states via transformations of the form

$$|1'\rangle=C_{11}|1\rangle+C_{31}|3\rangle\ , \quad (46)$$

$$|2'\rangle=|2\rangle\ , \quad (47)$$

$$|3'\rangle=C_{13}|1\rangle+C_{33}|3\rangle\ , \quad (48)$$

are not useful, as they are in the lambda and vee cases [40].

In all cases, we have referred to the atomic density matrix elements as follows. *The one-photon atomic coherences* are $\rho_{12},\rho_{21},\rho_{23},\rho_{32}$, the *two-photon atomic coherences* are ρ_{13},ρ_{31}, and *the populations* are $\rho_{11},\rho_{22},\rho_{33}$. The appropriateness of this terminology describing atomic density matrix elements as "n-photon atomic coherences" follows from an examination of the response of two- and three-level atoms prepared in phase-dependent initial states and considered as detectors of the EM field. For a two-level atom detector, Barnett and Pegg [43] show that the detector response associates the one-photon atomic coherences with the one-photon correlation functions for the field $\langle\hat{E}^{\pm}(t)\rangle$. For a three-level atom detector, Dalton and Knight [44] show that the detector response associates the two-photon atomic coherences with two-photon correlation functions for the field $\langle\hat{E}^{s}(t_1)\hat{E}^{r}(t_2)\rangle$ $(s,r=+,-)$.

The possible states of the atomic system are specified by the atomic density matrix and the five distinct types of states are illustrated in Fig. 9. Note that since the state may change with time, a state with two-photon coherence could become a state with a single one-photon coherence.

As we have seen in (41), the phase dependence of the variance of the source field quadrature component (and, of course, its time average) for the ladder system depends, in general, on both one-photon coherences and two-photon coherences. In other words, various types of source-field squeezing can be distinguished, depending on which coherences are nonzero for the source-field state in question. These are illustrated in Fig. 9 also.

In situations where squeezing occurs, we shall ascertain which atomic coherences are significant and designate the type of squeezing in accordance with Fig. 9. As we will see, two distinct types of squeezing occur in ladder systems.

C. Results

Our numerical studies are confined to the steady-state regime and based on Eqs. (43), (44), and (45) for the time-averaged normally ordered variance (NOV for short) of the optimally chosen quadrature component in units of κ^2 at appropriate quadrature frequencies, for both the ES

	State with:	Atomic Density Matrix	Types of Squeezing	Occurs for
A	Single One Photon Coherence	$\begin{pmatrix}\bullet & \bullet & 0\\ \bullet & \bullet & 0\\ 0 & 0 & \bullet\end{pmatrix}$ or $\begin{pmatrix}\bullet & 0 & 0\\ 0 & \bullet & \bullet\\ 0 & \bullet & \bullet\end{pmatrix}$	Two Level	Λ,V,Ξ
B	Pair of One Photon Coherences	$\begin{pmatrix}\bullet & \bullet & 0\\ \bullet & \bullet & \bullet\\ 0 & \bullet & \bullet\end{pmatrix}$	Two Level Pair	Λ,V,Ξ
C	Two Photon Coherence	$\begin{pmatrix}\bullet & 0 & \bullet\\ 0 & \bullet & 0\\ \bullet & 0 & \bullet\end{pmatrix}$	Three Level	Ξ
D	Two Photon Coherence and Single One Photon Coherence	$\begin{pmatrix}\bullet & \bullet & \bullet\\ \bullet & \bullet & 0\\ \bullet & 0 & \bullet\end{pmatrix}$ or $\begin{pmatrix}\bullet & 0 & \bullet\\ 0 & \bullet & \bullet\\ \bullet & \bullet & \bullet\end{pmatrix}$	Two Level-Three Level	Λ,V,Ξ
E	General Coherence	$\begin{pmatrix}\bullet & \bullet & \bullet\\ \bullet & \bullet & \bullet\\ \bullet & \bullet & \bullet\end{pmatrix}$	General	Λ,V,Ξ

FIG. 9. The distinct states and types of squeezing for three-level systems. A large dot indicates a nonzero density matrix element.

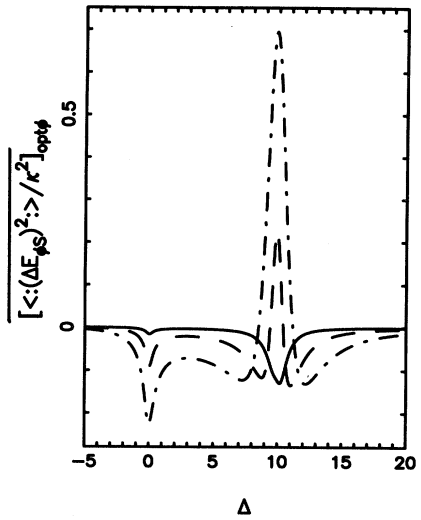

FIG. 10. The optimized normally ordered time-averaged variance $(\langle :\Delta\hat{E}^2_{\phi S}: \rangle /\kappa^2)_{\mathrm{opt}\phi}$ as a function of two-photon detuning Δ for the ES level case and the quadrature frequency $\omega=\omega_L$. The decay rates are $\gamma_1=\gamma_2=0.5$, coherence transfer rate $\gamma_{21}=0.5$, and the detuning $\delta=10$. Results for various equal Rabi frequencies $\xi_1=\xi_2=\xi$ are shown; $\xi=0.2$ (solid line), $\xi=0.5$ (dashed line), and $\xi=1.0$ (broken line).

and NES level cases. The results for the steady-state values of the density matrix elements are obtained from Eq. (A7).

Figure 10 shows the NOV versus two-photon detuning for the ES level case with quadrature frequency $\omega=\omega_L$ for the decay rates $\gamma_1=\gamma_2=0.5$, coherence transfer rate $\gamma_{21}=0.5$, detuning $\delta=10$, and various equal Rabi frequencies $\xi_1=\xi_2=\xi$. Here we see significant squeezing at $\Delta=0$, corresponding to zero two-photon detuning and near $\Delta=\delta$, corresponding to zero lower-transition one-photon detuning $\Delta_1=0$. The squeezing near $\Delta=0$ gets larger as the Rabi frequency increases, as does that near $\Delta=\delta$ for small Rabi frequencies. For larger Rabi frequencies, the squeezing near zero lower-transition one-photon detuning has a double minimum corresponding to the one-photon Rabi splitting of the dressed atom energy levels. Figure 11 shows the steady-state atomic coherences versus two-photon detuning for the same situation as in Fig. 10 and with Rabi frequency $\xi=1.0$. Thus we see that for the squeezing near $\Delta=0$, the two-photon coherent $|\sigma_{13}|$ is large, the one-photon coherence $|\sigma_{12}|$ is significant, but diminishing. This is a mixed situation of two-level–three-level squeezing. On the other hand, near $\Delta=\delta$ only the one-photon coherence $|\sigma_{12}|$ is large and this is a case of two-level squeezing.

The squeezing status near zero two-photon detuning changes significantly if we change the one-photon detuning and the Rabi frequency. Figure 12 shows the NOV versus two-photon detuning for the ES level case with quadrature frequency $\omega=\omega_L$, for the same decay and coherence transfer rates as in Fig. 10, but with detuning $\delta=500$ and with equal Rabi frequencies $\xi_1=\xi_2=\xi=5$. Again, squeezing occurs near $\Delta=0$. Figure 13 shows the

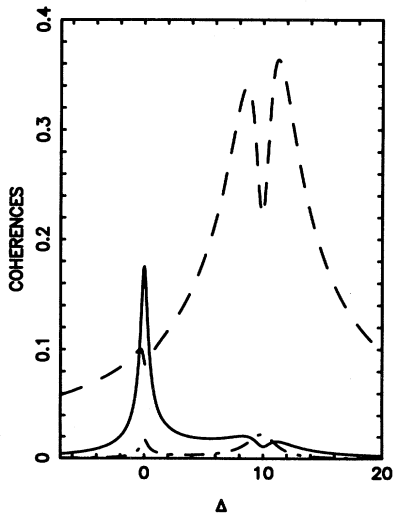

FIG. 11. The steady-state atomic coherences as a function of two-photon detuning Δ for the ES level case with decay rates $\gamma_1=\gamma_2=0.5$, coherence transfer rate $\gamma_{21}=0.5$, detuning $\delta=10$, and equal Rabi frequencies $\xi_1=\xi_2=\xi=1$. The coherence $|\sigma_{13}|$ is shown (solid line), $|\sigma_{12}|$ (dashed line), and $|\sigma_{23}|$ (broken line).

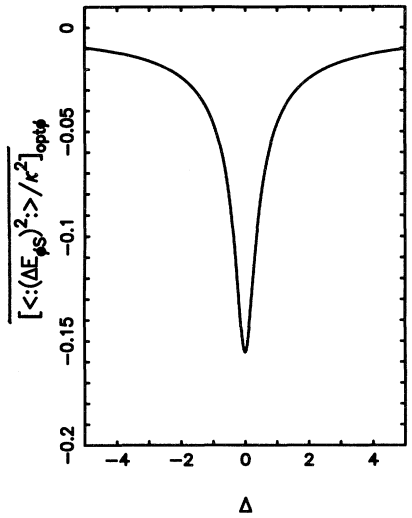

FIG. 12. The optimized normally ordered time-averaged variance $(\langle :\Delta\hat{E}^2_{\phi S}: \rangle/\kappa^2)_{\mathrm{opt}\phi}$ as a function of two-photon detuning Δ for the ES level case and for quadrature frequency $\omega=\omega_L$. The decay rates are $\gamma_1=\gamma_2=0.5$, coherence transfer rate $\gamma_{21}=0.5$, and the detuning $\delta=500$. The equal Rabi frequencies are $\xi_1=\xi_2=\xi=5$.

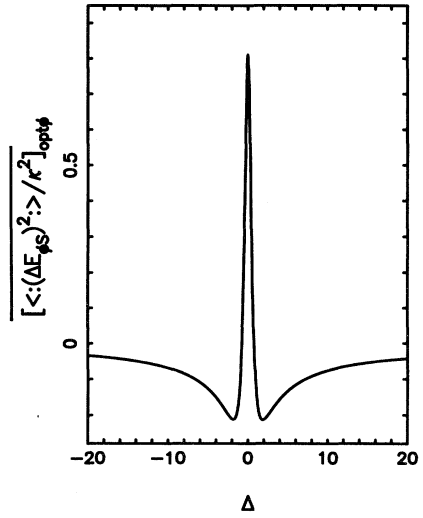

FIG. 14. The optimized normally ordered time-averaged variance $(\langle :\Delta\hat{E}^2_{\phi S}: \rangle/\kappa^2)_{\mathrm{opt}\phi}$ as a function of two-photon detuning Δ for the ES level case and for quadrature frequency $\omega=\omega_L$. The decay rates are $\gamma_1=\gamma_2=0.5$, coherence transfer rate $\gamma_{21}=0.5$, and the detuning $\delta=500$. The equal Rabi frequencies are $\xi_1=\xi_2=\xi=20$.

steady-state atomic coherences for the same situation as in Fig. 12. In this case, only the two-photon coherence σ_{13} is large near $\Delta=0$ and we essentially have a situation of three-level squeezing.

Figure 14 shows the NOV versus two-photon detuning for the same ES level case as in Fig. 12, but now with even larger Rabi frequencies $\xi_1=\xi_2=\xi=20$, though with the same one-photon detuning $\delta=500$. Here we see that the squeezing has a double minimum near $\Delta=0$ corresponding to a two-photon Rabi-frequency splitting of dressed atom levels based on $|1\rangle,|3\rangle$. In this case, the two-photon Rabi frequencies $\sim(20)^2/500\sim0.8$, so here we see the two-photon analogy of the splitting effect near $\Delta=\delta$ (zero one-photon detuning) seen in Fig. 10. Figure 15 shows the steady-state atomic coherences for the same situation as in Fig. 14. Again, only the two-photon coher-

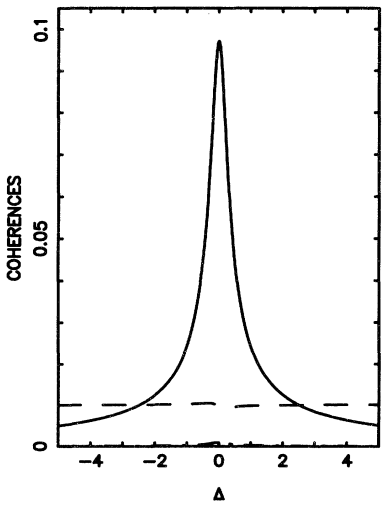

FIG. 13. The steady-state atomic coherences as a function of two-photon detuning Δ for the ES level case with decay rates $\gamma_1=\gamma_2=0.5$, coherence transfer rate $\gamma_{21}=0.5$, detuning $\delta=500$, and equal Rabi frequencies $\xi_1=\xi_2=\xi=5$. The coherence $|\sigma_{13}|$ is shown (solid line), $|\sigma_{12}|$ (dashed line), and $|\sigma_{23}|$ (broken line).

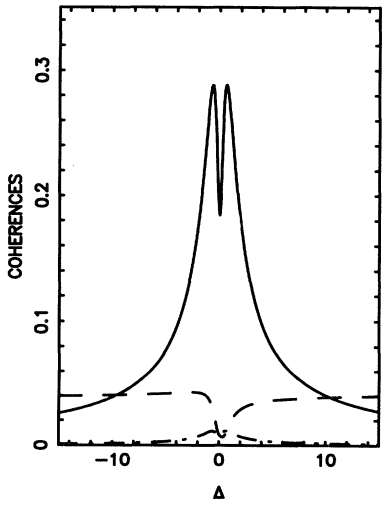

FIG. 15. The steady-state atomic coherences as a function of two-photon detuning Δ for the ES level case with decay rates $\gamma_1=\gamma_2=0.5$, coherence transfer rate $\gamma_{21}=0.5$, detuning $\delta=500$, and equal Rabi frequencies $\xi_1=\xi_2=\xi=20$. The coherence $|\sigma_{13}|$ is shown (solid line), $|\sigma_{12}|$ (dashed line), and $|\sigma_{23}|$ (broken line).

ence is large and we have a situation of three-level squeezing.

Figure 16 shows the NOV versus two-photon detuning for the NES case with quadrature frequency $\omega=\frac{1}{2}(\omega_a+\omega_b)$ for the decay rates $\gamma_1=\gamma_2=0.5$, coherence transfer rate $\gamma_{21}=0$, detuning $\delta=10$, and for various equal Rabi frequencies $\xi_1=\xi_2=\xi$. Here we see significant squeezing near two-photon resonance $\Delta=0$, which gets larger as the Rabi frequency increases. For the same situation as in Fig. 16 and with Rabi frequency $\xi=1.0$, Fig. 17 shows the steady-state atomic coherences versus two-photon detuning. Near the squeezing regime at $\Delta=0$ the two-photon coherence is large and the one-photon coherence $|\sigma_{12}|$ is still significant, but decreasing and the other one-photon coherence $|\sigma_{23}|$ is negligible. This situation is a mixed one of two-level–three-level squeezing. However, if the one-photon detuning and the Rabi frequency are altered, a situation of pure three-level squeezing can be obtained near zero two-photon detuning, just as for the ES level case. For example, the parameter choice $\gamma_1=\gamma_2=0.5$, $\gamma_{21}=0$, $\delta=500$, and $\xi_1=\xi_2=\xi=5$ produces, near $\Delta=0$, graphs similar to those shown in Figs. 12 and 13, and the parameter choice $\gamma_1=\gamma_2=0.5$, $\gamma_{21}=0$, $\delta=500$, and $\xi_1=\xi_2=\xi=20$ yields graphs almost the same as those presented in Fig. 14 and 15. In the interest of brevity, these graphs are not shown.

Squeezing properties of the fluorescence field for the NES case strongly depend on the quadrature frequency ω. Figure 18 shows the NOV versus two-photon detuning for the NES case but with quadrature frequency $\omega=\omega_a$, for the decay rates $\gamma_1=\gamma_2=0.5$, coherence transfer rate $\gamma_{21}=0$, detuning $\delta=10$, and various equal Rabi frequencies $\xi_1=\xi_2=\xi$. Again, we see significant squeezing around $\Delta=\delta$, corresponding to zero lower-transition one-photon detuning $\Delta_1=0$, but there is no squeezing near $\Delta=0$, zero two-photon detuning. For small Rabi frequencies the squeezing is largest at $\Delta=\delta$, whereas for larger Rabi frequencies the squeezing has a

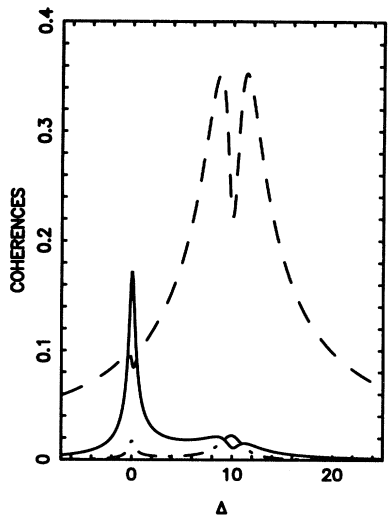

FIG. 17. The steady-state atomic coherences as a function of two-photon detuning Δ for the NES level case with decay rates $\gamma_1=\gamma_2=0.5$, coherence transfer rate $\gamma_{21}=0$, detuning $\delta=10$, and equal Rabi frequencies $\xi_1=\xi_2=\xi=1.0$. The coherence $|\sigma_{13}|$ is shown (solid line), $|\sigma_{12}|$ (dashed line), and $|\sigma_{23}|$ (broken line).

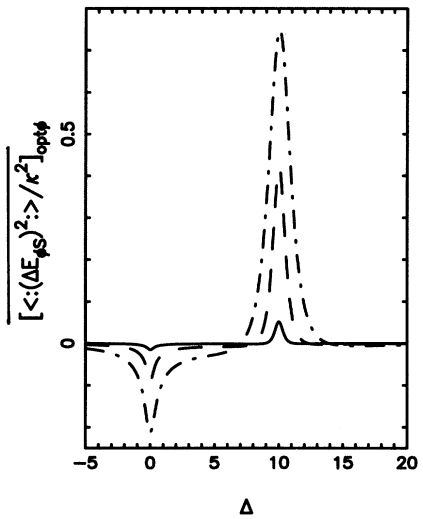

FIG. 16. The optimized normally ordered time-averaged variance $(\langle:\Delta\hat{E}^2_{\phi S}:\rangle/\kappa^2)_{\text{opt}\phi}$ as a function of two-photon detuning Δ for the NES level case and for quadrature frequency $\omega=\frac{1}{2}(\omega_a+\omega_b)$. The decay rates are $\gamma_1=\gamma_2=0.5$, coherence transfer rate $\gamma_{21}=0$, and the detuning $\delta=10$. Results for various equal Rabi frequencies $\xi_1=\xi_2=\xi$ are shown; $\xi=0.2$ (solid line), $\xi=0.5$ (dashed line), and $\xi=1.0$ (broken line).

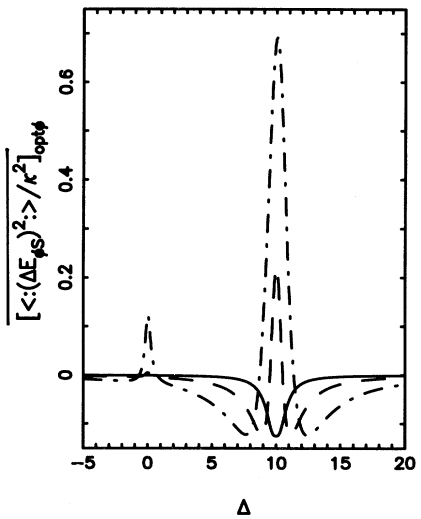

FIG. 18. The optimized normally ordered time-averaged variance $(\langle:\Delta\hat{E}^2_{\phi S}:\rangle/\kappa^2)_{\text{opt}\phi}$ as a function of two-photon detuning Δ for the quadrature frequency $\omega=\omega_a$ and for the NES level case. The decay rates are $\gamma_1=\gamma_2=0.5$, coherence transfer rate $\gamma_{21}=0$, and the detuning $\delta=10$. Results for various equal Rabi frequencies $\xi_1=\xi_2=\xi$ are shown; $\xi=0.2$ (solid line), $\xi=0.5$ (dashed line), and $\xi=1.0$ (broken line).

double minimum, corresponding to the Rabi splitting of the dressed atom energy levels. For $\xi=1$, the atomic coherences are as in Fig. 17 and we see that only $|\sigma_{12}|$ is large when squeezing occurs, indicating that the squeezing is of the two-level type.

In the present work, the largest squeezing obtained has $(\langle:\Delta\hat{E}^2_{\phi S}:\rangle/\kappa^2)_{\text{opt}\phi}\approx -0.2$ (see Fig. 14) for the regime of zero two-photon detuning, where the squeezing shows a predominantly three-level character. In our general study for the optimum squeezing in three-level systems [40] (and for which we also had $c=s=1/\sqrt{2}$), the optimum value of $(\langle:\Delta\hat{E}^2_{\phi S}:\rangle)/\kappa^2)_{\text{opt}\phi}$ was approximately -0.41. Although in this case purely three-level squeezing was obtained, the optimum value for squeezing was not, in fact, reached for the specific resonance fluoresence process and the parameter choices studied here.

It should be noted here that the squeezing properties near two-photon resonance are similar to the multiatom squeezed states recently discussed by Barnett and Dupertuis [32]. They have shown that two two-level atoms can radiate squeezed light even when the expectation values of the dipole moments are zero. This effect is due to a nonvanishing expectation value of the square of the collective atomic operators. In fact, the system of two two-level atoms, under some conditions [45–48], is equivalent to the three-level ladder system and the square of the collective atomic operators corresponds to the two-photon coherences.

V. SUMMARY

In this paper, we have studied the two-photon properties of resonance fluorescence emitted from a coherently excited three-level atoms with a ladder configuration of energy levels. In such a system, two-photon absorption greatly modifies the steady-state populations of the atomic levels and the atomic coherences. In particular, we have shown in the steady state that in addition to the well-known resonant behavior of the upper-state population centered on zero two-photon detuning, the intermediate state also exhibits the same resonance. This behavior changes the fluctuation properties of the fluorescent light and leads to unusual three-level squeezing properties near two-photon resonance. This squeezing is not present in the Λ- and V-type atoms, and is inherent three-level squeezing. Moreover, squeezing near two-photon resonance increases with the intensity of the driving field and attains its maximum value for moderate intensities and large one-photon detunings. This is in contrast to the squeezing behavior near one-photon resonance, where squeezing is largest for a weak driving field.

ACKNOWLEDGMENTS

This work was supported in part by the UK Science and Engineering Research Council and by the European Community. One of us (Z.F.) acknowledges the support of the Australian Research Council.

[1] T. Hänsch and P. Toschek, Z. Phys. **236**, 213 (1970).
[2] R. G. Brewer and E. L. Hahn, Phys. Rev. A **11**, 1641 (1975).
[3] R. M. Whitley and C. R. Stroud, Jr., Phys. Rev. A **14**, 1498 (1976).
[4] C. Cohen-Tannoudji and S. Reynaud, J. Phys. B **10**, 2311 (1977).
[5] R. Salomaa, J. Phys. B **10**, 3005 (1977).
[6] P. W. Milonni and J. H. Eberly, J. Chem. Phys. **68**, 1602 (1978).
[7] M. Takatsuji, Phys. Rev. A **11**, 619 (1975).
[8] K. Shimoda, Appl. Phys. **9**, 239 (1976).
[9] S. Stenholm, *Foundation of Laser Spectroscopy* (Wiley, New York, 1984), p. 150.
[10] M. D. Levenson and N. Bloembergen, Phys. Rev. Lett. **32**, 645 (1974).
[11] F. Biraben, B. Cagnac, and G. Grynberg, Phys. Rev. Lett. **32**, 643 (1974).
[12] C. C. Wang and L. I. Davis, Jr., Phys. Rev. Lett. **35**, 650 (1975).
[13] J. F. Ward and A. V. Smith, Phys. Rev. Lett. **35**, 653 (1975).
[14] D. Grischkowsky, M. M. T. Loy, and P. F. Liao, Phys. Rev. A **12**, 2514 (1975).
[15] N. Bloembergen and M. D. Levenson, in *High Resolution Laser Spectroscopy*, edited by K. Shimoda, Topics in Applied Physics Vol. 13 (Springer-Verlag, Berlin, 1976), p. 315.
[16] V.S. Letokhov and V. P. Chebotayev, in *Non Linear-Laser Spectroscopy*, edited by D. L. MacAdam, Springer Series in Optical Sciences Vol. 4 (Springer-Verlag, Berlin, 1977).
[17] M. D. Levenson and S. S. Kano, *Introduction to Non Linear Laser Spectroscopy* (Academic, New York, 1982).
[18] B. W. Shore, *Theory of Coherent Atomic Excitation* (Wiley, New York, 1990), Vols. 1 and 2.
[19] Z. Ficek and P. D. Drummond, Phys. Rev. A **43**, 6247, 6258 (1991); Europhys. Lett. **24**, 455 (1993).
[20] V. Buzek, P. L. Knight, and I. K. Kudryavtsev, Phys. Rev. A **44**, 1931 (1991).
[21] M. O. Scully, K. Wodkiewicz, M. S. Zubairy, J. Bergou, N. Lu, and J. M. ter Vehn, Phys. Rev. Lett. **60**, 1832 (1988).
[22] N. Lu, F.-X. Zhao, and J. Bergou, Phys. Rev. A **39**, 5189 (1989).
[23] N. A. Ansari and K. Zaheer, Opt. Commun. **92**, 79 (1992).
[24] J. Zakrzewski, M. Lewenstein, and T. W. Mossberg, Phys. Rev. A **44**, 7717 (1992); **44**, 7732 (1992); **44**, 7746 (1992).
[25] S. Swain, Physics World **5** (4), 25 (1992).
[26] D. J. Gauthier, Q. Wu, S. E. Morin, and T. W. Mossberg, Phys. Rev. Lett. **68**, 464 (1992).
[27] T. D. Kieu and B. J. Dalton, Opt. Acta **31**, 1307 (1984).
[28] W. Neuhauser, M. Hohenstatt, P. E. Toschek, and H. Dehmelt, Phys. Rev. A **22**, 1137 (1980).
[29] (a) L. Mandel, Phys. Rev. Lett. **49**, 136 (1982). (b) J. Mod. Opt. **34**, (6/7) (1987), special issues on squeezed light, edited by R. Loudon and P. L. Knight; (c) J. Opt. Soc. Am. B

4, (10) (1987), special issue on squeezed light edited by H. J. Kimble and D. F. Walls; (d) K. Zaheer and M. S. Zubairy, Adv. At. Mol. Phys. **28**, 142 (1991).
[30] M. J. Collett, D. F. Walls, and P. Zoller, Opt. Commun. **52**, 145 (1984).
[31] K. Wodkiewicz, P. L. Knight, S. T. Buckle, and S. M. Barnett, Phys. Rev. A **35**, 2567 (1987).
[32] S. M. Barnett and M. A. Dupertuis, J. Opt. Soc. Am. B **4**, 505 (1987).
[33] D. F. Walls and P. Zoller, Phys. Rev. Lett. **47**, 709 (1981).
[34] R. Loudon, Opt. Commun. **49**, 24 (1984).
[35] Z. Ficek, R. Tanas, and S. Kielich, J. Opt. Soc. Am. B **1**, 882 (1984).
[36] F. A. M. de Oliveira, B. J. Dalton, and P. L. Knight, J. Opt. Soc. Am. B **4**, 1558 (1987).
[37] W. Vogel and R. Blatt, Phys. Rev. A **45**, 3319 (1992).
[38] Z. Ficek, B. J. Dalton, and P. L. Knight, Phys. Rev. A **50**, 2594 (1994).
[39] P. A. Lakshmi and G. S. Agarwal, Phys. Rev. A **32**, 1643 (1985).
[40] B. J. Dalton, Z. Ficek, and P. L. Knight, Phys. Rev. A **50**, 2646 (1994).
[41] G. S. Agarwal, in *Quantum Optics,* edited by G. Höhler, Springer Tracts in Modern Physics Vol. 70 (Springer-Verlag, Berlin, 1974), p. 88.
[42] C. Cohen-Tannoudji, in *Frontiers in Laser Spectroscopy,* edited by R. Balian, S. Haroche, and S. Liberman (North-Holland, Amsterdam, 1977), p. 33.
[43] S. M. Barnett and D. P. Pegg, J. Phys. A **19**, 3849 (1986).
[44] B. J. Dalton and P. L. Knight, Phys. Rev. A **42**, 3034 (1990).
[45] R. H. Dicke, Phys. Rev. **93**, 99 (1954).
[46] R. H. Lehmberg, Phys. Rev. A **2**, 883 (1970).
[47] S. M. Barnett and P. L. Knight, Phys. Scr. **T21**, 5 (1988).
[] Z. Ficek and R. Tanas, in *Modern Nonlinear Optics, Part 1,* edited by M. Evans and S. Kielich (Wiley, New York, 1993), p. 461.
[48] Z. Ficek and R. Tanas, in *Modern Nonlinear Optics, Part 1,* edited by M. Evans and S. Kielich (Wiley, New York, 1993), p. 461.